Energy deposition at the divertor plates during elmy H-mode and poloidal and toroidal distribution of heat load on the wall inASDEX Upgrade

A. Herrmann, P. Franzen, W. Herrmann, C.F. Fuchs, M. Weinlich, ASDEX Upgrade team, NI-team, ICRH-team

Max-Planck-Institut für Plasmaphysik, EURATOM Association, Garching and Greifswald; Germany

Introduction

A crucial problem of future nuclear fusion reactors is the power handling. The operation of the next step tokamak ITER demands the handling of about 300 MW α-particle power crossing the separatrix. An additional difficulty arises from the envisaged H-mode operation, because this confinement regime is accompanied by edge localized modes (ELMs) which cause short lasting high power pulses across the separatrix which may be intolerably high. The energy transport due to ELMs and it's dependence on local and global plasma parameters has been carefully investigated in the ASDEX Upgrade tokamak. Additionally, the poloidal and toroidal distribution of the heat load of the inner walls of ASDEX Upgrade was measured time integrated by cooling water calorimetry.

Energy deposition to the divertor plates during elmy H-mode

One topic of this paper is the energy deposition onto the inner and outer divertor of ASDEX Upgrade during elmy H-mode phases as measured by thermography [1]. The time resolution of the thermography system is 260 μs/line and the spatial (radial) resolution is 2.7 mm/pixel and 3.2 mm/pixel for the outer and inner Divertor plates, respectively.

In a first step, the frequency behaviour of the power deposition to the inner plate was characterized by continuous wavelet analysis [2]. It was found, that there are qualitatively two classes for the frequency behaviour of type-I ELMs - periodic and aperiodic. For periodic ELMs the frequency is constant if the discharge conditions are unchanged. Aperiodic ELMs show a variation of the ELM frequency by a factor of up to two, though the global discharge conditions are kept constant.

Both types of ELM-behaviour are under investigation in this paper but the energy deposition to the inner and outer plate as well as the ELM-frequency are time averaged over about 20 ELM periods. The deposited energy is the sum of the deposition to the inner and outer plate, whereas the ratio inner to outer plate is about 3.

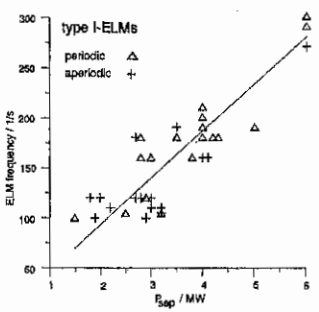

Fig. 1: The ELM frequency increase with the heating power.

Figure 1 shows the increase of the ELM-frequency with the power crossing the separatrix, P_{Sep}, as it is typical for type-I ELMs. A linear fit through the origin gives: $f_{ELM}(Hz) \sim 50 \times P_{Sep}(MW)$.

The energy deposited per ELM varies between 2 and 10 kJ/ELM and shows a tendency to increase with P_{Sep}. The energy loss in the midplane calculated from the electron temperature and the density profile measured in the midplane by Thomson scattering and Lithium beam, respectively, is about a factor of two higher (10–20 kJ/ELM) [3].

The fraction of power transported by an

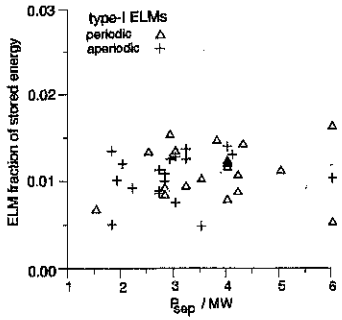

Fig. 2: The fraction of stored energy deposited per ELM to the target plates is between 1-2%

ELM, $\frac{\Delta W^{target}_{ELM} \cdot f_{ELM}}{P_{sep}}$, is in the order of 30%. This value is independent of P_{scp} and comparable to values of other tokamaks [4]. The same statement holds for the fraction of stored energy, $\frac{\Delta W^{target}_{ELM}}{W_{plasma}}$ which is in the order of 1–2 %, as shown in figure 2. The data under consideration are taken from low radiating discharges with $P_{sep} = (0.5 \pm 0.1) \times P_{in}$. From this and from the fact, that the fraction of transported power as well as the fraction of stored energy is constant follows that the ELM frequency is inverse proportional to the energy confinement time.

The constant ratio of the stored energy deposited per ELM to the target plates and the fact, that the temperature profiles are self-similar for a wide range of parameters [5], which is found from ECE measurements, implies that the energy extraction depth is independent of the heating power and depends only from the density profile. There is no significant difference in energy deposition for periodic and aperiodic ELMs.

Consequences for ITER. The value for the fraction of stored energy, which is comparable for ASDEX and JET [4], can be used to estimate the ELM effects on the divertor for ITER conditions. Assuming a heating power of $P_{in} = 300$ MW, and an energy confinement time of $\tau_e = 6$ s the stored energy is W = 1.8 GW and the energy loss per ELM transported to the divertor, $\Delta W = 0.02$–0.04 GW.

The deposition area is calculated from the major radius and a power decay length scaling derived for ASDEX Upgrade H-mode discharges [6], $\lambda_p^{target}(mm) = 6.36 \times 10^{-3} P_{sep}^{0.52} q_{95}^{0.7}$. With $\lambda_p^{target}(150MW, 3) \simeq 0.3m$ and $R_0 = 8.14m$ the deposition area is: $A_{dep} \simeq 30m^2$. Using this value the energy density at the target plate per ELM becomes, $w = (0.7 - 1.2)\frac{MWs}{m^2}$.

The uncertainty in this estimation is the contribution of the ITER geometry. While the fraction of stored energy is found to be constant for different tokamaks at about the same value, the decay length scaling is limited to ASDEX Upgrade data. If the major radius is a hidden parameter, the scaling should be modified to: $\lambda_p^{target}(mm) = \left(\frac{R_0^{ITER}}{R_0^{AUG}}\right)^{\alpha} \lambda_p^{target,AUG}$, with $\frac{R_0^{ITER}}{R_0^{AUG}} = \frac{8.14}{1.65} = 4.93$, resulting in $w = (4.93)^{-\alpha}(0.7 - 1.2)\frac{MWs}{m^2}$. If e.g. the power decay length scales with P_{sep}/R_0, α becomes -0.52 and w increases by a factor of 2.3.

Wether or the high energy density can be tolerated depends on the caused temperature increase, which is given by: $\Delta T = \frac{w}{\sqrt{\Delta t}} \frac{2}{\sqrt{\pi}} \frac{1}{\sqrt{\kappa \rho c_p}}$. With a heat conduction of, $\kappa = 1.2\frac{W}{cmK}$, and a product of density and specific heat of, $\rho c_p = 3.6\frac{Ws}{cm^3 K}$, which are typical for CFC-material envisaged for ITER divertor plates, the maximum temperature becomes: $\Delta T(K) = 58 \times \frac{w\left(\frac{MWs}{m^2}\right)}{\sqrt{\Delta t(s)}}$. The resulting temperature increase for a temporal ELM-width of Δt=1 ms, and α=0 is: $\Delta T = (1300 \div 2200)K$

This values are at the limit but depend on some uncertain values as α, and the ELM duration which may change the value for the temperature increase. If elmy H-mode is an operation scenario for ITER further on, the decay length scaling found on ASDEX Upgrade should be checked at other tokamaks.

Poloidal and toroidal distribution of heat load

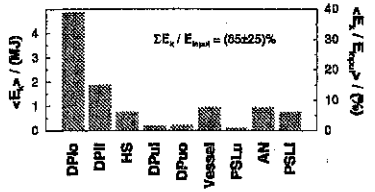

Fig. 3: Mean poloidal distribution of heat load in ASDEX Upgrade for normal operation conditions — single null neutral beam heated low radiative elmy H-mode discharges without disruptions. The acronyms are explained in the text.

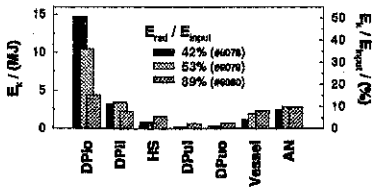

Fig. 4: Poloidal distribution of heat load in ASDEX Upgrade in dependence on the radiated energy fraction for three discharges with otherwise equal plasma parameters. At the time of these discharges, the heat load on both PSL was measured not yet. The acronyms are explained in the text.

Cooling water calorimetry. The cooling water calorimetry system at ASDEX Upgrade (CWC) measures the heat load on the inner wall tiles (and the vacuum vessel) poloidally and toroidally resolved, from the integrated temperature difference of inlet and return water temperature and the water flow rate. For each of the main component (lower outer (DPlo), lower inner (DPli), upper inner (DPui), and upper outer (DPuo) divertor plates and the inner heat shield (HS), respectively) a measuring device for each torus sector is installed. With the additionally measuring devices at the lower and upper stabilizing loops (PSLl, PSLu), ICRH antennas (AN) and the vacuum vessel, CWC covers more than 90% of the ASDEX Upgrade inner wall. The fraction of the energy measured by CWC to the total input energy - which should be unit - amounts to (85±25)%. The large scatter is due to radiation and charge exchange losses through ports which are not covered by CWC.

Poloidal distribution. Figure 3 shows the mean poloidal distribution of the heat load for discharges with normal operation conditions, i.e. single null neutral beam heated elmy H-mode discharges without disruptions and radiated energy fractions below 68 %. In this case, the lower outer divertor plates receive between 30 % and 40 % of the total input power, resulting in heat loads of up to 1 MJ per sector for discharges with 10 MW additional heating power. For the normal conditions, the inner divertor tiles receive about 15 % of the input energy. Between 5 % and 10 % of the input energy is deposited on the inner heat shield, the vacuum vessel, lower PSL and the ICRH antennas, whereas the heat load on the upper divertor and PSL is negligible. The heat load on the outer divertor tiles can be reduced by radiation in the plasma mantle by a factor of about 3 (fig. 4), with only a minor reduction of the heat load on the inner divertor tiles. Due to the increased radiation, the heat loads on the other inner wall components also increase, but this increase cannot account for the decrease of the divertor heat load due to loss channels not covered by CWC. The heat load on the outer divertor tiles is also reduced for L-mode and/or disruptive discharges, and discharges with the ion ∇B drift towards the upper divertor plates.

Toroidal distribution. Figure 5. shows as an example the mean toroidal distribution of the heat load on the outer divertor tiles. As can be seen, the distribution is asymmetric, the maximum values exceed the mean value by more than 15 %; however, the position of the maxima depends on the discharge conditions, especially on the direction of the ion ∇B drift. For the case of normal operation, i.e. $I_p > 0$ and $B_t < 0$, the direction of the ion ∇B drift is towards the lower divertor plates, and the maximum heat loads are on the tiles in sectors 10 to 13, whereas in the case of the ion ∇B drift towards the upper divertor plates, i.e. $I_p > 0$ and $B_t > 0$, the maximum heat loads are on the tiles in sectors 2 to 4. Apparently, the distribution exhibits a dominant n = 1 structure with a smaller n = 2 distribution. The depen-

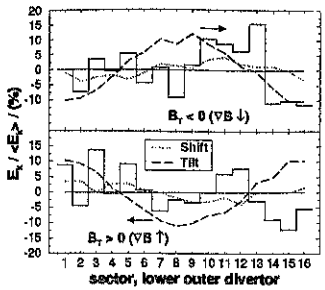

Fig. 5: Toroidal distribution of heat load in ASDEX Upgrade for normal operation conditions (see figure 3). The dashed and dotted lines show results of field line calculations (see text). The arrow denotes the direction of the shift of the maximum due to transport perpendicular to the field lines.

dence of the heat load distribution on the ion ∇B drift, and not on the sign of the magnetic field, is confirmed by discharges with counter NI injection (i.e. $I_p < 0$), where in the case of $B_t > 0$ the same distribution as in the case of $I_p > 0$ and $B_t < 0$ shows up. The measured asymmetry in the heat load distribution on the lower outer divertor plates is consistent with other toroidal asymmetries observed in ASDEX Upgrade. After the start of neutral injection, where the separatrix position was not much changed, a colored ring was observed at the outer divertor plates. The center of this ring was shifted against the geometrical axis in direction of sector 13. Similar observations were made by Langmuir probes in sectors 4 and 13: the separatrix positions differ by about 10 mm, also indicating a shift towards sector 13. Furthermore, all locked modes lock also in sector 13, as observed by the Mirnov coils. All these observations indicate that the magnetic axis of the magnetic field coils is somewhat misaligned to the geometrical axis of the vacuum vessel. In order to get some hints on the nature of the misalignment, we performed field line calculations, assuming that the radial transport in the midplane is symmetric and that the heat load on the targets is proportional to the field line density, for two scenarios with a n = 1 distortion: (a) a shift of the geometric axis of 5 mm towards sector 13, and (b) tilting the geometric axis in such a way that also a shift of 5 mm at the outer target plates results. Both scenarios reproduce the shift of the separatrix position very well; they also reproduce rather the heat load maximum position (see figure 5) as well as the dependence on the ion ∇B drift direction, if one considers the shift of the maximum heat load due to transport perpendicular to the field lines. However, only scenario (b) - which is technically the more improbable - also reproduces the amount of the maximum heat load enhancement. Hence, the observed toroidal asymmetries cannot be explained solely by geometrical effects, but other distortions play a role also, so perhaps a distortion of the magnetic field in the midplane by a not complete compensation of the iron yokes and the magnets of the neutral beam injection box located in sector 13. As a consequence for the ITER design, small distortions and misalignment of the magnetic structure can enhance the heat load on some special locations of the divertor by 10 % to 20 %, neglecting geometrical effects.

References

[1] A. Herrmann, W. Junker, K. Günther et al., Plasma Phys. Control. Fusion 37 (1995) 17
[2] V. Dose, G. Venus, H. Zohm, Phys. Plasmas 4(1997) 323
[3] H. Reimerdes, IPP-Report 1/300, p.57
[4] J. Lingertat, 4th European Fusion Physics Workshop, Stockholm, 11-13 December 1996
[5] W. Suttrop, Joint U.S.-European Transport Task Force Workshop, Madison WI, April 23-26, 1997
[6] A. Herrmann, M. Laux, O. Kardaun et al., 23rd EPS conference on Contr. Fusion and Plasma Phys. II d039 (1996)